Boosting the short-circuit current density of organic photovoltaics using a composite electrode

Boosting the short-circuit current density of organic photovoltaics using a composite electrode

S. Saylan[a,*], C. T. Howells[b]

[a] *Masdar Institute, Khalifa University of Science and Technology, Abu Dhabi, United Arab Emirates*

[b] *KAUST Solar Center (KSC), Physical Sciences and Engineering Division (PSE), King Abdullah University of Science and Technology (KAUST), Thuwal 23955-6900, Kingdom of Saudi Arabia*

Abstract

Progress in organic photovoltaic (OPV) efficiency is key to low-cost energy production. Device architectures comprising of the most effective materials, morphology, and well-designed layouts sit alongside the strategy which targets low-cost and high-performance devices. Here we report, an enhancement of the short-circuit current density, a key performance parameter, by using a silver/aluminum composite electrode in OPVs with a regular architecture. The use of the composite electrode in the inverted architecture results in a substantially reduced silver electrode thickness and thus offers material cost reductions. This work also highlights the importance of modeling the interference effects for optimizing the layer thicknesses along with systematic optimization of materials, morphology, and interfaces to further the enhancements in the field. For example, by simply reducing the thickness of the commonly used ZnO and MoO_3 interlayers in an inverted OPV it is possible to improve the short-circuit density. The optical field intensity distributions and optical power confinement within the active layer are exploited to reveal the origin of this enhancement.

Keywords: `Photovoltaic`, Composite electrode, Transfer matrix method (TMM), Optical interference

2010 MSC: 00-01, 99-00

*Corresponding author

Email address: `ssaylan@masdar.ac.ae` (S. Saylan)

1. Introduction

The architecture of an organic photovoltaic (OPV) cell plays an important role in the efficiency. Optimization of the architecture requires a systematic approach and understanding of the optical and electrical behavior of the layers of organic and inorganic materials. The selection of materials and thicknesses thereof should allow for an optimum electromagnetic field distribution, and thus strong absorption of solar irradiation, accompanied by efficient exciton dissociation, charge transport and extraction. Work on enhanced energy harvesting efficiency with the use of highly reflective electrodes has been reported [1, 2].

It is well-known that efficient charge separation in bulk heterojunction OPVs depends on the difference between the LUMOs and HOMOs for dissociation in the donor and acceptor, respectively. Furthermore, the open circuit voltage (V_{OC}) is related to the difference between the HOMO of the donor and the LUMO of the acceptor, and the metal work-function does not play a critical role on the open circuit voltage for ohmic contacts [2–5]. The regular architecture employs indium tin oxide (ITO) and aluminum (Al) as the anode and cathode, respectively. A low work-function metal such as calcium, barium, lithium, or magnesium may be deposited prior to the aluminum, depending on the electron acceptor material of interest, to ensure an ohmic contact [6–9]. However, this is known to degrade the device stability due to the high reactivity of these metals [3]. Efforts towards replacing low work-function reactive metals with air-stable transition metal oxides has led to the development of inverted organic photovoltaic devices [3]. Furthermore, interlayers have been introduced into both regular and inverted OPVs so as to perform specific functions such as modifying the work-function of the electrodes and form Ohmic contacts for optimal charge extraction, forming electron or hole selective contacts, modifying the optical field, and protecting the underlying active layer.

Effective charge collection in the organic solar cells predominately relies on the hole and electron extraction layers, which reside between the photoactive

layer and electrodes, as well as the formation of Ohmic contacts for effective charge extraction. Two examples of mostly used anode interlayers are poly(3,4 ethylenedioxythiophene):poly(styrenesulfonate) (PEDOT:PSS) and metal oxides such as MoO_3, WO_3 and V_2O_5 [10–13]. In the past, the metal-oxides suffered the disadvantage of requiring high temperature vacuum processing and post-deposition annealing, being incompatible with the solution-processable, large-area, high-throughput, and cost-effective targets of OPVs. In this respect, there is some promise in recent advancements in the development of solution-processed metal-oxide films [14, 15]. Moreover, high refractive index metal oxides such as MoO_3 may cause parasitic reflection at the ITO interface [1] due to the impedance mismatch [16, 17] between the ITO and metal-oxide. Optical losses in metal-oxides are not limited to reflection; parasitic absorption in these layers at short wavelengths can also be significant [1]. On the other hand, OPVs fabricated using solution-processed MoO_3 have demonstrated better stability than the devices with PEDOT:PSS [18], which may facilitate degradation of OPV stability and lifetime. Recently, it has been demonstrated that, by using the anionic perfluorinated ionomer (PFI) as additives to PEDOT:PSS, both the stability and lifetime can be improved [9].

Our interest in OPVs originates from low-cost high-throughput processing. Materials and processing costs are influenced by the scale of production. Krebs and co-workers demonstrated for current (kW regime), upscaled (100 MW regime) and industrial production, the use of Ag is an unacceptable cost [19]. In summary, the cost of processing is about 15% of the overall cost to produce an OPV today. This decreases as one scales up the production. For commercially available P3HT:PCBM OPVs 33% of the cost is for Ag. The active layer consisting of both donor and acceptor materials amounts to 13% of the total cost. The interlayers, adhesives, and solvents cost 12%. The remaining cost, which makes majority of the total cost for this regime is for the barrier foil, i.e., 42%. However, if production is upscaled or industrialized the cost of the barrier foil decreases by half and the dominate cost is the Ag at 46 or 51%, respectively. The cost of the active layer is 19% for upscaled and 11% for industrialized pro-

duction. There is almost no difference in the total cost of the other materials, 15% compared to 17%, respectively. In the study, a cost reduction of 77% for the electrodes by using Al instead of Ag is reported. This makes sense as the cost for a gram of Ag is around 30 times that of Al. Therefore, reducing the thickness of Ag, maintaining all the advantages Ag has over Al, i.e., stability, reflectance, etc., is of interest.

In this paper, regular and inverted architectures are revisited with a focus on the choice of metal electrode, looking for a highly reflective, electrically compatible, and cost-effective alternative. We note that the photoactive blend poly(3-hexylthiophene-2,5-diyl):[6,6]-phenyl-C61-butyric acid methyl ester (P3HT:$PC_{61}BM$) is used for both regular and inverted architectures. The optical field intensity distribution within the active layer, obtained using a transfer matrix code [16, 20], is used to estimate the theoretical absorption of the cell. We first investigate the use of the composite electrode, based on a thin Ag film capped by Al, in comparison to the Al cathode in the regular architecture, utilizing a stack of ITO/PEDOT:PSS/photoactive-blend/cathode. We show that the use of composite metal electrode, along with optimized interlayer thicknesses, provides an opportunity of short circuit current density (J_{SC}) enhancement. It is worth to briefly mention that high V_{OC} cells have been demonstrated previously using a PCDTBT:$PC_{70}BM$ bulk heterojunction active layer and Ag electrode [21]; it was found that the devices with Ag, Ca, Ca/Ag, and Ca/Al cathodes yielded similar V_{OC} of around 0.85 V, despite the differences in the work-function. On the contrary, V_{OC} obtained with the Al cathode was limited to 0.78 V. The similarity of V_{OC} obtained with different cathode materials implies the formation of an ohmic contact as explained earlier. Given that the electron accepting fullerene in our study, as in [21], is PCBM, we anticipate an ohmic contact to be formed between the P3HT:$PC_{61}BM$ and Ag/Al composite cathode. In addition to enhancing the J_{SC}, the composite Ag/Al electrode provides an advantage with respect to the device stability by avoiding the use of reactive metals such as Ca. In another study, using the regular architecture based on the P3HT:$PC_{61}BM$ blend and Ag cathode, it was shown that the

removal of low work-function metal, such as Ca, did not compromise the V_{OC} or FF [1]. In the study, the efficiency determining parameter was thus mainly J_{SC}. Investigations with pentacene-C_{60} heterojunction solar cells yielded results comparable to those obtained for the P3HT:$PC_{61}BM$ blend; similar V_{OC} was obtained with Ag and Al cathodes, it being slightly higher for Ag [2]. Combined with an enhanced J_{SC} as indicated by our results, these suggest that the use of Ag/Al composite electrode in a regular architecture may lead to high efficiency heterojunction solar cells based on different photoactive layers.

We also focus on the exploitation of the composite electrode as a substitute for the Ag anode in the inverted architecture, where we consider commonly favored MoO_3 and ZnO as hole extraction and electron extraction layers, respectively [3, 22–25]. For the case of an inverted OPV, where Ag is the commonly favoured anode [22–25], the composite electrode offers significant cost reduction as discussed above. Furthermore, we provide the results of modeling showing the device performance based on varying ZnO thickness in the inverted architecture. Our findings, as also suggested previously [1, 21], show the importance of modeling the optical interference effects to determine the optimum thickness of the layers in an OPV, presenting a case that should also be considered when exploring new materials.

2. Materials and methods

The power absorbed in a layer can be expressed by the equation $A(\omega) = \omega \times Im(\epsilon) \int_V |E|^2 \, dV$ where ω is the angular frequency, $Im(\epsilon)$ is the imaginary part of the dielectric constant, E is the local electric field, and the integration volume is the volume of the layer [26]. The power confined in the layer is proportional to the integral term in this equation [27]. Thus, an architecture with improved confinement within the photoactive blend would increase absorption and hence the J_{SC}. The optical electrical field distribution inside the multilayer stack of an OPV, due to a normally incident plane wave, can be calculated as a function of position using the transfer matrix method followed by Peumans et

al. [20]. We have applied the same formalism, to calculate the power absorbed and J_{SC} generated by an OPV device where the recombination losses are negligible, by using the complex index of refraction for the materials; either obtained from the literature [28, 29] or experimentally, as in the case of glass, Al, ITO, PEDOT:PSS, and P3HT:PCBM, using a spectroscopic ellipsometer (M-2000 from J.A. Woollam Co., Inc.). For the calculation of J_{SC}, we assume lossless diffusion, dissociation of excitons, and collection of the free charge carriers at the electrodes.

3. Results and discussion

First, we model the Ag/Al composite electrode in the regular architecture, glass/ITO (100 nm)/PEDOT:PSS(40 nm)/P3HT:PCBM/cathode, varying the P3HT:PCBM thickness between 40 and 100 nm. The dependence of J_{SC} on the thickness of Ag in a Ag/Al(200-nm-thick) composite is plotted in Fig. 1 for different thicknesses of P3HT:PCBM. As seen from the figure, a 80-nm-thick P3HT:PCBM provides the highest J_{SC} for the entire Ag thickness range, including the case of an aluminum-only cathode. For this optimum P3HT:PCBM thickness, a composite electrode of Ag(30-nm-thick)/Al(200-nm-thick) offers a 5% increase in J_{SC} compared to a 200-nm-thick Al only contact, as presented in the inlay of Fig. 1. The enhancement may be attributed to an electrode with a reflectivity greater than that of Al at the wavelengths which the active layer absorbs. These results indicate that there is value in modeling the optical interference effects when new materials are investigated to ensure the thickness of the active layer is tuned for maximal absorption before other factors are investigated.

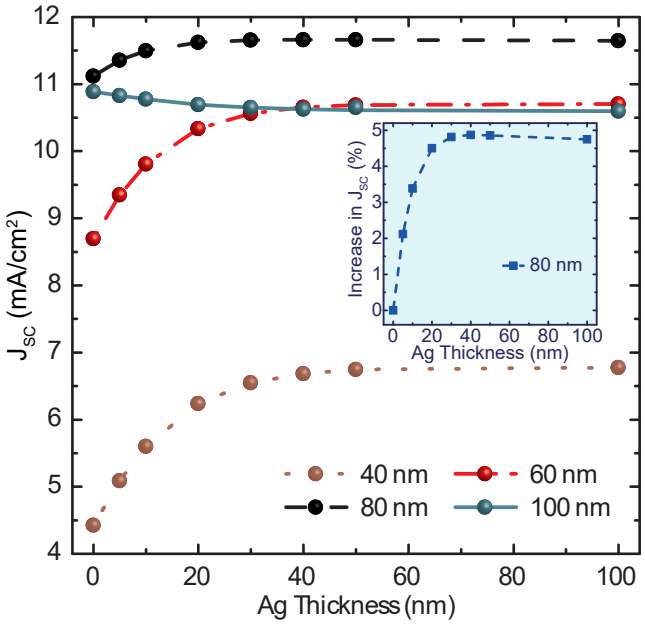

Figure 1: Dependence of J_{SC} on the thickness of Ag in an Ag/Al composite electrode, plotted for different thicknesses of P3HT:PCBM. The inlay shows the increase in J_{SC} for the optimum P3HT:PCBM thickness (80 nm) as a function of Ag thickness.

Next, we implement the Ag/Al composite electrode in an inverted architecture with a typical composition, that is, glass/ITO(100 nm)/ZnO/P3HT:PCBM (80 nm)/MoO_3/anode, where we, like so many others, assume an optimal 40-nm- and 10-nm-thick ZnO and MoO_3 film [24, 25], respectively, as well as a 200-nm-thick Ag anode for the baseline. Furthermore, we investigate the short-circuit current density dependence on ZnO thickness. Figure 2 shows the J_{SC} calculated for the inverted devices with varying ZnO thickness comprising the Ag(30-nm-thick)/Al(200-nm-thick) electrode, in comparison to the baseline device modeled using an Ag only anode. The influence of the 10-nm-thick MoO_3 interlayer is also presented for the two anode configurations. It is apparent that the J_{SC} drops as the ZnO thickness is increased beyond about 20 nm for each scenario. Moreover, for both anode configurations, i.e., conventional and the composite, the J_{SC} improves when the MoO_3 is not used. Although the

composite electrode produces similar levels of J_{SC} as the conventional, with and without the MoO_3 interlayer, in the case of composite electrode it is possible to reduce the cost of materials by reducing the amount of silver used in the anode to around 30 nm. To evaluate the performance of the optimized design, in comparison to the baseline structure defined above, we calculate the increase in J_{SC} as given in the right axis of Fig. 2. These results show that an OPV device with the Ag(30-nm-thick)/Al(200-nm-thick) electrode and about 20-nm-thick ZnO as the cathode interfacial layer, not comprising a MoO_3 anode interfacial layer, offers about 9.5% increase in the J_{SC} compared to the baseline architecture, which represents a notable improvement.

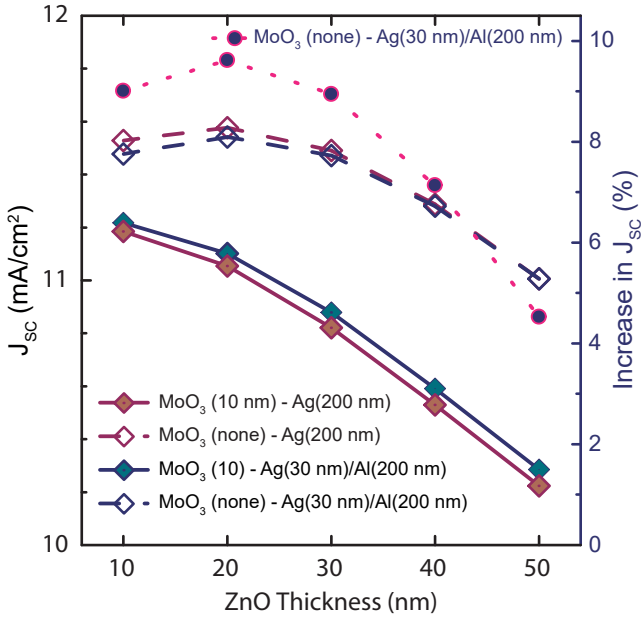

Figure 2: Left axis plots the dependence of J_{SC} on the thickness of ZnO for the two cases of Ag-only and Ag/Al composite anode, with (10-nm-thick) and without a MoO_3 anode interfacial layer. Right axis plots the increase in J_{SC} with the Ag(30 nm)/Al(200 nm) electrode, in the absence of the MoO_3 layer, in comparison to the baseline device architecture.

To further elucidate the reasoning behind the above-mentioned 9.5% enhancement in J_{SC}, we modeled the optical field intensity distribution $|E|^2$ inside

the photoactive P3HT:PCBM film for the associated architectures, which is plotted in Fig. 3(b)-(d) at three different wavelengths of λ=350, 450, and 550 nm. The architectures labelled as A1 and A2 in Fig. 3 are glass/ITO(100 nm)/ZnO (40 nm)/P3HT:PCBM(80 nm)/MoO_3(10 nm)/Ag(200 nm) and glass/ITO(100 nm)/ZnO(20 nm)/P3HT:PCBM(80 nm)/Ag(30 nm)/Al(200 nm), respectively. As depicted in Fig. 3(a), the power absorbed by the 80-nm-thick photoactive layer in architecture A2 supersedes the one in architecture A1 for the entire spectrum from 300 to around 600 nm, thus leading to a notable increase in the short-circuit current density for this architecture. Optical power confined in the photoactive layer is proportional to the area under the optical field intensity graph [27]. The areas under the field intensity graphs given in Fig. 3(b)-(d) are integrated along the active layer and plotted as a function of depth (cathode interface is at x=0 and x=80 corresponds to the anode interface) in the layer in Fig. 3(e)-(g). In agreement with the absorbance spectrum, the integrated area is higher for architecture A2 at all three wavelengths, i.e., λ=350, 450, and 550 nm. Therefore, the increase in J_{SC} with architecture A2 is due to the increased absorption by the photoactive layer resulting from an enhanced optical power confinement inside this layer.

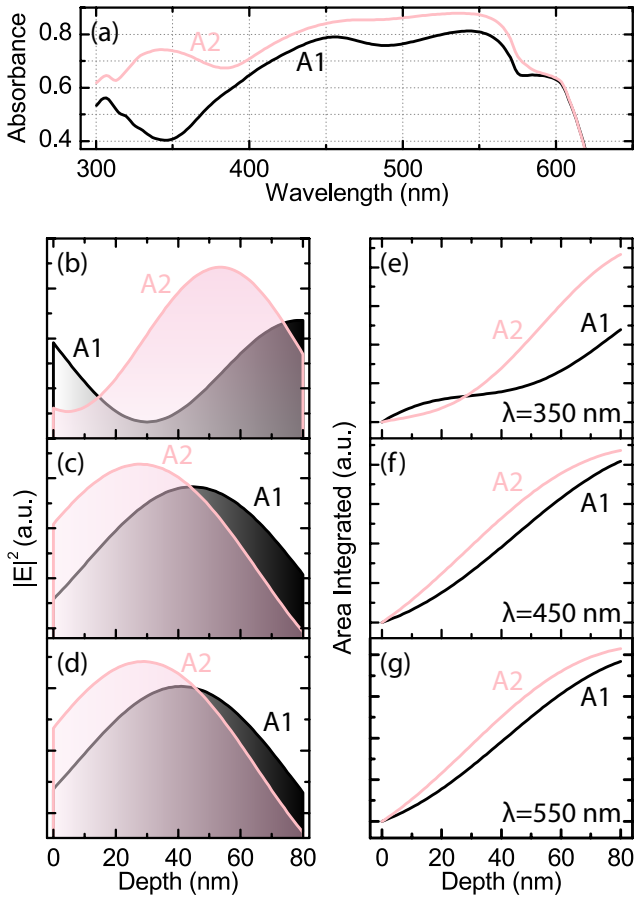

Figure 3: Power absorbed by the 80-nm-thick photoactive (P3HT:$PC_{61}BM$) layer, along with the optical field intensity distribution $|E|^2$ inside the layer and the area under the field intensity plots integrated and plotted along the layer. A1 and A2 represent the following device architectures respectively: glass/ITO(100 nm)/ZnO(40 nm)/P3HT:PCBM(80 nm)/MoO_3(10 nm)/Ag(200 nm) and glass/ITO(100 nm)/ZnO(20 nm)/P3HT:PCBM(80 nm)/Ag(30 nm)/Al(200 nm). The wavelength of the incident light is λ=350, 450, and 550 nm, respectively, in (b)/(e), (c)/(f), and (d)/(g).

As we have demonstrated in Fig. 2, the J_{SC} of an inverted OPV with 80-nm-thick P3HT:PCBM improves notably with the removal of the MoO_3. However, the use of an interlayer at the anode may be unavoidable for efficient carrier extraction. In the literature, it has been demonstrated that, by form-

ing an ohmic contact at the organic and metal interface, the addition of a 2-nm-thick NiO improves the V_{OC} and FF of an inverted cell based on the P3HT:PCBM blend and Ag anode [30]. This provides the motivation for investigating how the absorbance of the photoactive layer would be influenced by depositing some of the mostly used interlayers [3] such as PEDOT:PSS or NiO of less than 5 nm thickness prior to the Ag(30-nm-thick)/Al(200-nm-thick) electrode. The absorbance calculated for the OPV structure of ITO(100 nm)/ZnO(20 nm)/P3HT:PCBM(80 nm)/interlayer/composite-electrode is presented in Fig. 4 for a wavelength range of 300-650 nm, where the interlayer is PEDOT:PSS, NiO, or MoO_3. Modeling of an OPV with 10-nm-thick MoO_3 and without an interlayer have also been presented for comparison. As seen from the figure, the absorbance remains almost the same with the addition of an interlayer, for the materials and thicknesses considered, in the wavelengths above 400 nm, except for the 10-nm-thick MoO_3. This explains the difference in J_{SC} observed in Fig. 2 with and without the 10-nm-thick MoO_3 interlayer. The loss in the absorbance observed at the wavelengths below 400 nm can be considered as insignificant due to the reduced photon flux in the Air Mass (AM)1.5G solar spectrum for these wavelengths. Moreover, as it has been reported for an inverted architecture based on the P3HT:PCBM blend and Ag anode, a V_{OC} of the same value can be attained with MoO_3 anode interlayers with the thickness ranging between 1 and 20 nm. The authors attributed the lower FF at MoO_3 thicknesses less than 10 nm to a limited amount of damage associated with the Ag electrode deposition. Therefore, if the damage during electrode deposition can be prevented, by employing an interlayer of a few nanometers per se, it may be possible to achieve high performance with an improved FF and J_{SC}.

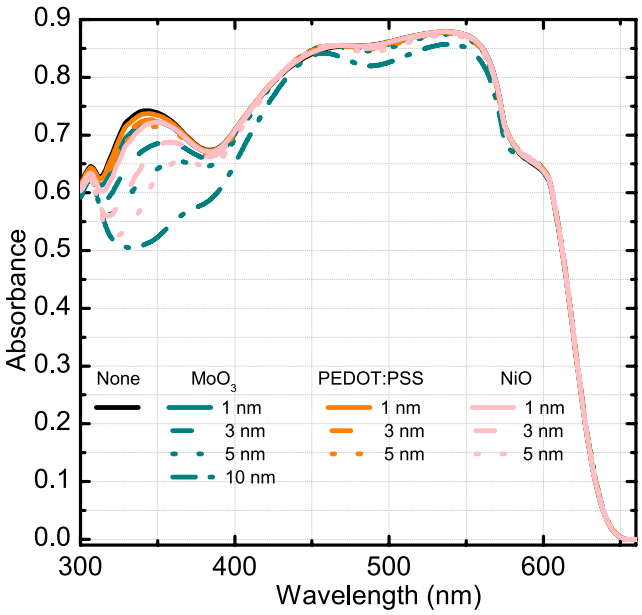

Figure 4: Power absorbed by the 80-nm-thick photoactive (P3HT:PCBM) layer, as calculated for an inverted OPV, considering various buffer materials atop the composite anode of Ag(30 nm)/Al(200 nm) in comparison to the case where a buffer layer is omitted.

4. Conclusion

We propose a composite electrode based on two of the most widely used metals, that is, a thin film of Ag capped by Al, for enhanced performance and/or reduced material costs in OPV. Through optical modeling of a regular OPV, we demonstrate that it offers an enhanced short-circuit current density compared to an Al electrode when employing a P3HT:$PC_{61}BM$ photoactive layer. The maximum improvement is around 5% and this is with a composite electrode comprised of a 30-nm-thick Ag and 200-nm-thick Al. Though the enhancement maybe considered small, it is worth mentioning that the onset of absorption for P3HT:PCBM is around 650 nm and that the improved reflectivity of Ag over Al occurs at 500 nm. A considerable dip in reflectivity of Al is observed between 650 and 900 nm, the minima at 800 nm. It may be possible to achieve a greater than 5% enhancement with high performance OPV materials that ab-

sorb in the near-infrared, provided that the light is not completely absorbed by the active layer during the first pass (see Supporting Information for results of modeling based on the PTB7-Th(PCE10):IEICO-4F and PM6:Y6 blends). We further show that the thickness of layers should be optimized in an OPV—the photoactive layer thickness to begin with—in order to fully perceive the influence of a new concept and/or material. Our findings reveal that, in an inverted architecture based on the P3HT:$PC_{61}BM$ photoactive layer, the amount of Ag used can be reduced by employing the composite electrode. As indicated by our results, an inverted OPV with a 30-nm-thick Ag combined with a 200-nm-thick Al can deliver a short-circuit current density similar to that of a device with 200-nm-thick Ag. Based on the above, it is clear that the composite electrode offers an advantage with regards to material costs. We have demonstrated that the current density can be improved, both for the composite and the Ag-only electrodes, by removing the MoO_3 interlayer, i.e., 9.5%. But, this remains a significant challenge considering the requirements for efficient carrier extraction. Yet, the optical modeling conducted using some of the commonly preferred interlayers, including MoO_3, reveals that the composite electrode performs equally well with and without these interlayers when the interlayer thickness is limited to less than around 5 nm. There is evidence of an improvement in the short-circuit current density, with reduced thickness of ZnO at the cathode in a range of 10 to 50 nm. The modeling of interference effects in an OPV is essential for driving enhanced performance – our findings on the optimized ZnO thickness is a case in point. More work is clearly necessary to experimentally implement the Ag/Al composite electrodes into the regular and inverted architectures, and this work intends to present the potential offered by the composite electrode and provide insights into the application thereof in bulk heterojunction organic solar cells.

Acknowledgements

We thank Masdar Institute, Khalifa University of Science and Technology for funding this work.

References

[1] A. Hadipour, D. Cheyns, P. Heremans, B. P. Rand, Advanced Energy Materials 1 (5) (2011) 930–935.

[2] A. K. Pandey, P. E. Shaw, I. D. W. Samuel, J.-M. Nunzi, Applied Physics Letters 94 (10) (2009) 103303.

[3] G. Li, R. Zhu, Y. Yang, Nature Photonics 6 (3) (2012) 153.

[4] C. J. Brabec, A. Cravino, D. Meissner, N. S. Sariciftci, T. Fromherz, M. T. Rispens, L. Sanchez, J. C. Hummelen, Adv. Funct. Mater. 11 (5) (2001) 374.

[5] V. D. Mihailetchi, P. W. M. Blom, J. C. Hummelen, M. T. Rispens, Journal of Applied Physics 94 (10) (2003) 6849.

[6] D. Cortizo-Lacalle, C. T. Howells, U. K. Pandey, J. Cameron, N. J. Findlay, A. R. Inigo, T. Tuttle, P. J. Skabara, I. D. Samuel, Beilstein Journal of Organic Chemistry 10 (1) (2014) 2683.

[7] G. J. Hedley, A. J. Ward, A. Alekseev, C. T. Howells, E. R. Martins, L. A. Serrano, G. Cooke, A. Ruseckas, I. D. Samuel, Nature communications 4 (2013) 2867.

[8] C. T. Howells, K. Marbou, H. Kim, K. J. Lee, B. Heinrich, S. J. Kim, A. Nakao, T. Aoyama, S. Furukawa, J.-H. Kim, E. Kim, F. Mathevet, S. Mery, I. D. W. Samuel, A. A. Ghaferi, M. S. Dahlem, M. Uchiyama, S. Y. Kim, J. W. Wu, J.-C. Ribierre, C. Adachi, D.-W. Kim, P. André, Journal of Materials Chemistry A 4 (11) (2016) 4252.

[9] C. T. Howells, S. Saylan, H. Kim, K. Marbou, T. Aoyama, A. Nakao, M. Uchiyama, I. D. W. Samuel, D.-W. Kim, M. S. Dahlem, P. André, Journal of Materials Chemistry A 6 (33) (2018) 16012.

[10] K. Kawano, R. Pacios, D. Poplavskyy, J. Nelson, D. D. Bradley, J. R. Durrant, Solar energy materials and solar cells 20 (2006) 3520–3530.

[11] S. Chen, X. Yu, M. Zhang, J. Cao, Y. Li, L. Ding, G. Shi, Journal of Materials Chemistry A 20 (2015) 3520–3530.

[12] T. W. Lee, Y. Chung, O. Kwon, J. J. Park, Advanced Functional Materials 17 (3) (2007) 390–396.

[13] H. Kim, S.-H. Bae, T.-H. Han, K.-G. Lim, J.-H. Ahn, T.-W. Lee, Nanotechnology 25 (1) (2013) 014012.

[14] D. Ouyang, Z. Huang, W. C. Choy, Solution-processed metal oxide nanocrystals as carrier transport layers in organic and perovskite solar cells, Advanced Functional Materials 29 (1) (2019) 1804660.

[15] W. C. Choy, D. Zhang, Solution-processed metal oxides as efficient carrier transport layers for organic photovoltaics, Small 12 (4) (2016) 416–431.

[16] S. Saylan, T. Milakovich, S. A. Hadi, A. Nayfeh, E. A. Fitzgerald, M. S. Dahlem, Solar Energy 122 (2015) 76.

[17] S. L. Chuang, Physics of photonic devices, Vol. 80, John Wiley & Sons, 2012, Ch. 6.

[18] C. Girotto, E. Voroshazi, D. Cheyns, P. Heremans, B. P. Rand, Solution-processed moo3 thin films as a hole-injection layer for organic solar cells, ACS applied materials & interfaces 3 (9) (2011) 3244–3247.

[19] F. Machui, M. Hösel, N. Li, G. D. Spyropoulos, T. Ameri, R. R. Søndergaard, M. Jørgensen, A. Scheel, D. Gaiser, K. Kreul, D. Lenssen, Energy & Environmental Science 7 (9) (2014) 2792–2802.

[20] P. Peumans, A. Yakimov, S. R. Forrest, Journal of Applied Physics 93 (7) (2003) 3693.

[21] D. C. Watters, J. Kingsley, H. Yi, T. Wang, A. Iraqi, D. Lidzey, Organic Electronics 13 (8) (2012) 1401–1408.

[22] D. Chen, C. Zhang, T. Heng, W. Wei, Z. Wang, G. Han, Q. Feng, Y. Hao, J. Zhang, Japanese Journal of Applied Physics 54 (4) (2015) 042301.

[23] M. S. White, D. C. Olson, S. E. Shaheen, N. Kopidakis, D. S. Ginley, Appl. Phys. Lett. 3 (36) (2006) 18380–18383.

[24] C. Sprau, F. Buss, M. Wagner, D. Landerer, M. Koppitz, A. Schulz, D. Bahro, W. Schabel, P. Scharfer, A. Colsmann, Energy & Environmental Science 8 (9) (2015) 2744.

[25] D. Baran, N. Gasparini, A. Wadsworth, C. H. Tan, N. Wehbe, X. Song, Z. Hamid, W. Zhang, M. Neophytou, T. Kirchartz, C. J. Brabec, J. R. Durrant, I. McCulloch, Nature communications 9 (1) (2018) 2059.

[26] A. P. Vasudev, J. A. Schuller, M. L. Brongersma, Optics Express 20 (S3).

[27] B. E. A. Saleh, M. C. Teich, Fundamentals of Photonics, 2nd Edition, John Wiley & Sons, Hoboken, New Jersey, 2007, Ch. 8, pp. 303–305.

[28] R. J. Powell, W. E. Spicer, Physical Review B 2 (6) (1970) 2182.

[29] C. Stelling, C. Singh, M. Karg, T. A. König, M. Thelakkat, M. Retsch, Scientific reports 7 (2017) 42530.

[30] W. Yu, L. Shen, S. Ruan, F. Meng, J. Wang, E. Zhang, W. Chen, Solar Energy Materials and Solar Cells 98 (2012) 212.